International Journal for Multidisciplinary Research (IJFMR)
E-ISSN: 2582-2160 ● Website: www.ijfmr.com ● Email: editor@ijfmr.com

Simulation-Based Performance and Sensitivity Analysis of a Hybrid Solar–Piezoelectric Energy Harvesting System for Low-Power Traffic-Light Applications

Lennox Sitoloma[1], Godfrey Zulu[2], Wana Ngala[3], Ebenezer Kawana[4], Brian Halubanza[5]

[1,2,3,4,5]School of Engineering and Technology, Mulungushi University, Kabwe, Zambia

Abstract

This study evaluates a proposed solar–piezoelectric energy harvesting supply for a low-power traffic-light demonstrator using switching-level MATLAB/Simulink representations and a separate reduced-order battery-charging model. A 6 V, 2 W photovoltaic source, nominal 3.7 V, 2.2 Ah lithium-ion storage and an illustrative 0.225 W load are considered. Photovoltaic-only charging from 50% to 97% state of charge requires 15.01, 4.71 and 2.80 h at constant irradiances of 200, 600 and 1000 W/m², respectively, with the load disconnected. When hypothetical net piezoelectric inputs of 100 mW are applied at the battery boundary, the corresponding modelled charging-time reductions are 26.8%, 10.3% and 6.4%; inputs of 1 mW or less yield reductions below 0.5%. A one-at-a-time sensitivity analysis identifies the fitted photovoltaic current as a major determinant of charging time. These are conditional model outputs, not experimentally verified piezoelectric generation or evidence of practical roadway autonomy. The study provides quantitative thresholds for future transducer characterization and controlled photovoltaic-only versus hybrid comparisons. Reproducibility is limited by unavailable executable model files, incomplete solver settings and an idealized piezoelectric power interface.

Keywords: Solar–piezoelectric energy harvesting; simulation-based feasibility; photovoltaic charging; battery state of charge; sensitivity analysis; low-power traffic-light supply.

1. Introduction

Traffic light systems are essential to modern transportation infrastructure because they regulate vehicular and pedestrian movements and support safe and efficient traffic flow. However, conventional systems depend heavily on the national electrical grid and predetermined timing sequences. In developing regions characterized by frequent power outages, load shedding, and voltage fluctuations, this dependence can compromise reliability, causing congestion, delays, confusion, and increased accident risks [11].

Renewable energy technologies offer an alternative for improving traffic-light energy independence. Solar photovoltaic (PV) systems can support standalone operation without continuous grid dependence [12], [13], [14]. However, PV generation is intermittent because it depends on solar irradiance and

environmental conditions, making adequate energy storage necessary for operation during low irradiance and nighttime periods [15].

Piezoelectric energy harvesting provides a complementary renewable-energy source by converting mechanical deformation and vibration into electricity. In transportation environments, vehicle and pedestrian movements can provide mechanical excitation for piezoelectric transducers [16], [17], [18]. Although individual piezoelectric elements generate relatively small amounts of energy, appropriately configured arrays can provide supplementary power for low-power applications.

Prior work has investigated solar-powered traffic signals [12]–[14], piezoelectric harvesting [16]–[18], and hybrid solar–piezoelectric concepts [21]-[22], [26]. However, adding a secondary harvesting source does not itself establish a meaningful system-level energy benefit. A relevant engineering question is the minimum average net PZT power delivered to storage needed to change battery charging performance under different solar irradiance conditions. This study addresses that question through simulation-based scenario and parameter sensitivity analyses. The approach is a comparative modelling study, not experimental validation or a claim of a novel hybrid architecture. Recent pavement-focused reviews discuss the importance of realistic mechanical loading, packaging and power-management interfaces [28]. The objectives are to (i) estimate PV-only charging and load effects across irradiance scenarios, (ii) compare PV-only operation with hypothetical PV-plus-PZT net-power scenarios, and (iii) quantify sensitivity to selected model assumptions. The research question is whether a plausible supplementary power level materially changes predicted charging time, and how that change compares with PV and charger uncertainties. All reported findings are simulated or calculated; physical verification is reserved for future work.

2 Component Selection

The following component ratings define the simulated system architecture and nominal electrical assumptions. They are not presented as experimental results or independently verified hardware performance.

2.1 Solar Photovoltaic Panel

A 6 V, 2 W solar photovoltaic panel was selected as the primary energy-harvesting source because the proposed prototype has a relatively low electrical power requirement. Under ideal sunlight conditions, the theoretical current produced by the panel can be estimated from the fundamental relationship between electrical power, voltage, and current:

$$P_{PV} = V_{PV} I_{PV}$$

Consequently, the theoretical current is given by

$$I_{PV} = \frac{P_{PV}}{V_{PV}}$$

Substituting the rated values of the selected panel gives

$$I_{PV} = \frac{2}{6} = 0.333\ A$$

The rated current is approximately 0.33 A. The panel was selected as the intended primary energy source for the low-power demonstrator. The PZT array was included as a secondary source whose net energy contribution requires measurement.

2.2 Piezoelectric Array

Nine 27 mm PZT piezoelectric discs were selected as the secondary energy-harvesting source. The piezoelectric elements were configured in a three-series, three-parallel (3S3P) arrangement. The selection of this configuration was intended to provide an appropriate balance between the voltage and current characteristics required by the subsequent power-conditioning stage.

A nominal nine-disc 3S3P arrangement motivates the proposed secondary source. The charging-time study does not resolve disc mechanics, capacitance, impedance or rectifier losses; instead, it sweeps specified net average PZT power at the battery input. Thus the reported power scenarios are assumptions, not predicted output of nine physical discs.

2.3 Rectifier and Filtering Circuit

The output of the piezoelectric array is alternating and therefore requires rectification before it can be used for battery charging. A bridge rectifier was selected to convert the AC output of the PZT array into a unidirectional electrical output. A 470 µF smoothing capacitor was incorporated after the rectification stage to reduce voltage fluctuations and smooth the rectified waveform.

The conceptual PZT pathway includes rectification, filtering and isolation. No measured conversion efficiency is available; the reduced-order sensitivity model therefore defines PZT power at the battery boundary, after any hypothetical conditioning losses. A physically realizable charger and source-isolation interface remains to be developed and validated.

2.4 Charge Controller

The reduced-order PV path represents a TP4056-type constant-current/constant-voltage lithium-ion charger [23] with a 4.0–8.0 V input window, nominal 1 A current limit, 4.2 V regulation and termination near one-tenth of the programmed current. A 4.05 V restart threshold and simplified dropout behaviour are modelling assumptions rather than verified settings of a particular board.

No MPPT controller is modelled as the baseline. Claims regarding practical charger superiority are excluded because controller efficiency and implementation losses have not been independently validated.

2.5 Lithium-Ion Battery

A 3.7 V, 2.2 Ah lithium-ion battery was selected as the energy-storage component. The battery provides an energy buffer between the intermittent renewable-energy sources and the electrical load. This is particularly important because photovoltaic generation varies with solar irradiance, while piezoelectric generation depends on the occurrence and intensity of mechanical excitation.

The nominal energy storage capacity of the battery can be estimated using

$$E_{bat} = V_{bat} C_{bat}$$

where E_{bat}represents the nominal stored energy in watt-hours, $V_{bat}$is the nominal battery voltage, and $C_{bat}$is the battery capacity in ampere-hours. Therefore,

$$E_{bat} = 3.7 \times 2.2$$

which gives

$$E_{bat} = 8.14\ Wh$$

The nominal battery energy is 3.7 V × 2.2 Ah = 8.14 Wh. This nameplate calculation is not equivalent to usable battery energy, and the modelled state-of-charge trajectory depends on the assumed voltage–SOC curve and efficiency.

2.6 DC–DC Boost Converter

The conceptual architecture includes a step-up stage to supply a nominal 5 V traffic-light load. The switching-level model uses 40 kHz PWM, unlike the commercial MT3608 switching frequency of

approximately 1.2 MHz [24]; consequently the simulated voltage behaviour cannot be interpreted as validation of that specific commercial module.

The MT3608 switches at a fixed 1.2 MHz, whereas the Simulink model used a PWM boost stage at 40 kHz. In the simulated system, the converter produced an output voltage within approximately 5.09–5.11 V, indicating that a boost stage of this kind can hold a voltage close to the required 5 V rail.

The importance of efficient low-voltage power conversion is particularly relevant to the piezoelectric subsystem because energy harvested from low-power sources can be significantly affected by losses within the conditioning circuitry. Previous studies have therefore investigated self-starting boost converters capable of operating from input voltages of only a few hundred millivolts [9], [10], and [19].

2.7 Arduino Uno Rev 3 and Traffic-Light Load

A fixed-sequence Arduino-and-LED traffic-light demonstrator provides the motivating application. For the reduced-order simulation the complete electrical demand is idealized as a constant 0.225 W load; state-dependent LED consumption, controller startup and switching transients are not resolved.

The simulated application is a low-power demonstrator rather than a full-scale intersection traffic signal. Traffic sensing, adaptive timing and real roadway demand are outside the study scope.

The system architecture provides the basis for the scenario comparisons below; no physical test results are used as evidence in this article.

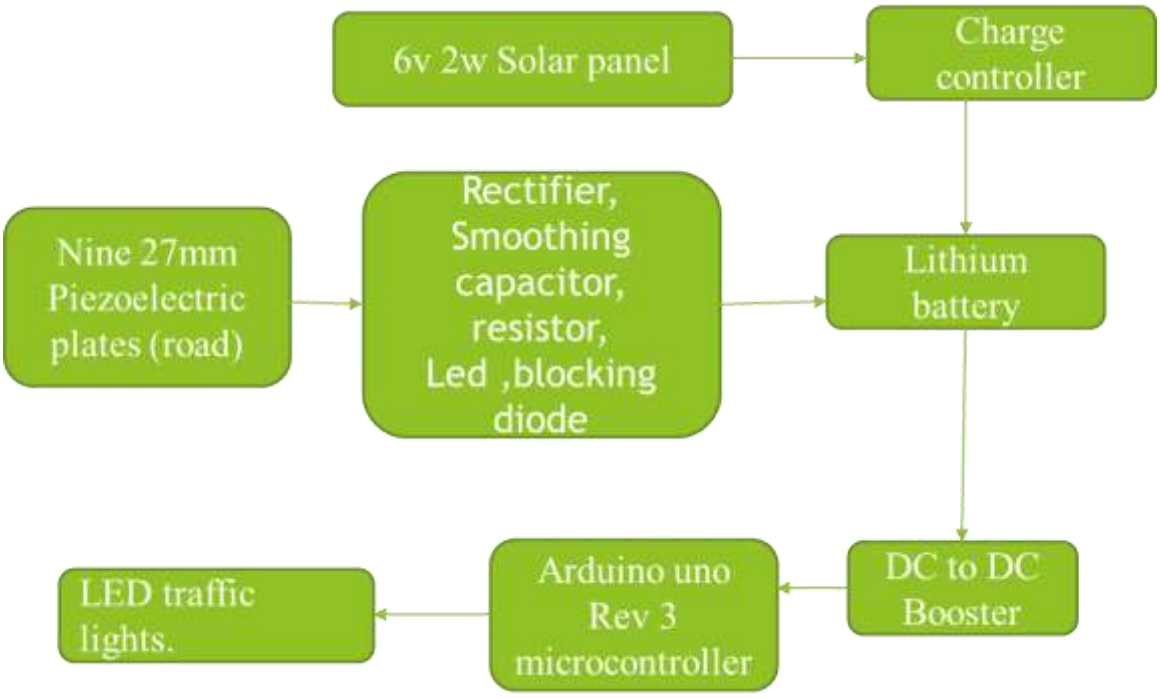


Figure 1. Conceptual architecture of the modelled PV–PZT battery-supported traffic-light supply (not a verified electrical schematic).

3. Methods

3.1 Simulation Setup

The modelling study uses two levels of representation. A MATLAB/Simulink 2024a switching-level system contains a PV block, idealized pulsed PZT voltage source, battery and 40 kHz boost stage with approximately 111 Ω load; irradiance scenarios are 100, 200, 600 and 1000 W/m² at 25 °C. The pulsed

PZT source is not calibrated to mechanical force or traffic. To simulate hours-long charging, a separate reduced-order model uses a single-diode PV I–V approximation (7.2 V open circuit, 0.38 A short circuit and approximately 2 W at 6 V under 1000 W/m²), a TP4056-type charging law, 3.7 V/2.2 Ah battery, initial 50% SOC, 97% SOC target, 10 s integration step and assumed boost efficiency of 0.85. The PV fit was estimated from plotted block characteristics and can deviate by about 16%. The reduced-order model treats PZT as an assumed average net power entering the battery. The two models are complementary and their results should not be presented as a single validated switching-level simulation. Complete source files, solver details and waveform parameters were not supplied. The reported hour-scale charging results originate from the reduced-order model rather than a continuous multi-hour switching-level simulation. The idealized PZT input represents net power at the battery boundary and therefore must not be equated with mechanical input or raw transducer output. A 40 kHz simulated boost stage is not a component-accurate model of the nominal 1.2 MHz MT3608 device. The charger re-start threshold and 85% boost efficiency are assumptions, not measured or datasheet-verified operating-point values.

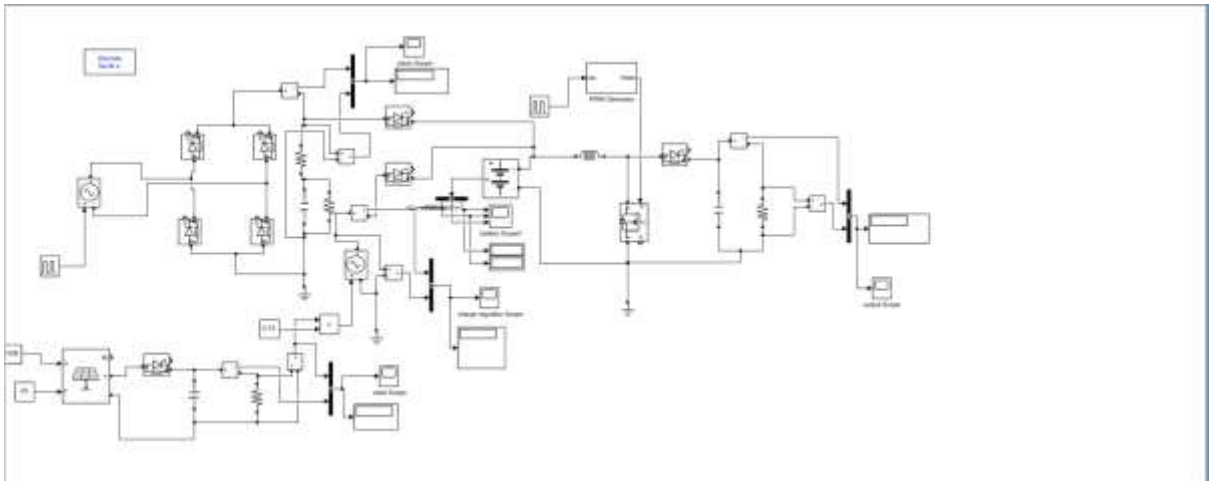


Figure 2. Original MATLAB/Simulink conceptual model; the separate reduced-order charging calculations underpin the hour-scale results.

4.1 Simulated PV-Only Charging and Load Dependence

Table 1 reports modelled PV operating points and charging times for irradiances of 100, 200, 600 and 1000 W/m². With the load disconnected, the simulated battery reaches 97% SOC after 33.0, 15.0, 4.71 and 2.80 h, respectively. With a constant 0.225 W load, the battery does not reach the target within 200 h at 100 or 200 W/m², while the corresponding times are 6.81 and 3.42 h at 600 and 1000 W/m². These are deterministic scenario outputs, not forecasts of field charging under time-varying sunlight.

Table 1. Simulated PV-only charging from 50% to 97% SOC under a TP4056-type model (original simulation values).

Irradiance (W/m²)	PV open-circuit voltage (V)	PV current at battery voltage (A)	Time to 97%, load off (h)	Time to 97%, load on (h)	Net energy in 2 h, load off (Wh)	Net energy in 2 h, load on (Wh)
100	5.9	0.031	33.0	never	0.241	−0.290
200	6.3	0.069	15.0	never	0.531	0.000

Irradiance (W/m²)	PV open-circuit voltage (V)	PV current at battery voltage (A)	Time to 97%, load off (h)	Time to 97%, load on (h)	Net energy in 2 h, load off (Wh)	Net energy in 2 h, load on (Wh)
600	6.9	0.221	4.71	6.81	1.702	1.167
1000	7.2	0.373	2.80	3.42	2.889	2.350

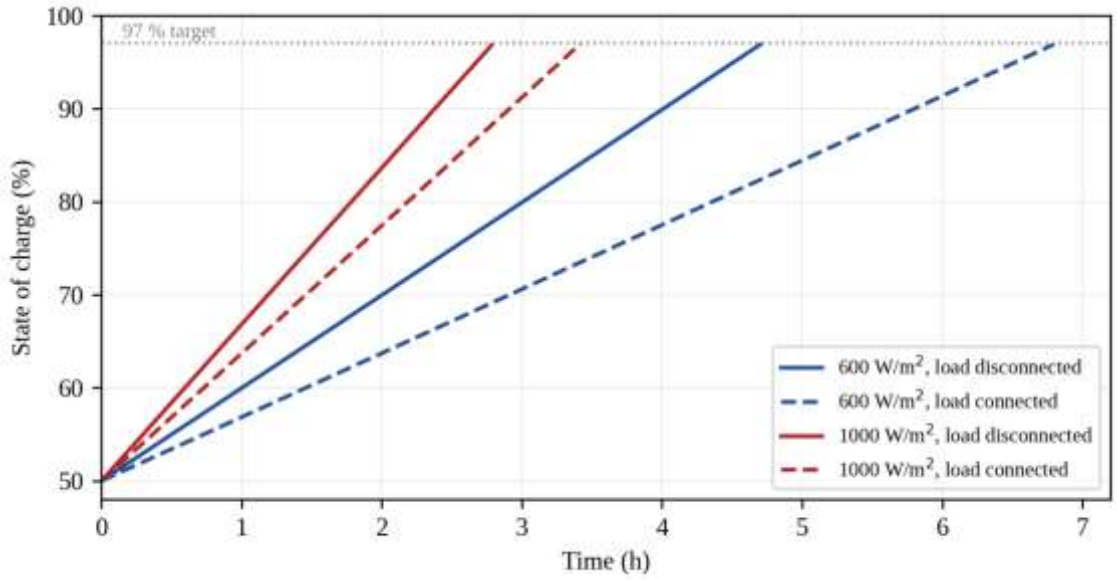


Figure 3. Simulated PV-only SOC trajectories at 600 and 1000 W/m² with load disconnected and connected.

The hypothetical PZT source is compared with PV-only charging at identical irradiance, initial SOC and charging interface, with the load disconnected. At assumed net PZT inputs of 100 mW, the simulated charging-time reductions are 26.8%, 10.3% and 6.4% at 200, 600 and 1000 W/m². At 10 mW the reductions are 3.5%, 1.1% and 0.7%; at 1 mW or below they are below 0.5%. These comparisons isolate a mathematical supplementary-power effect. They do not establish that the specified disc array can deliver the assumed net power or that a direct battery interface is safe or efficient.

Table 2. Simulated charging-time sensitivity to assumed net PZT power at the battery input (load disconnected).

PZT average power to battery	200 W/m²: time (h)	200 W/m²: reduction (%)	600 W/m²: time (h)	600 W/m²: reduction (%)	1000 W/m²: time (h)	1000 W/m²: reduction (%)
0 (PV only)	15.01	–	4.71	–	2.80	–
10 µW	15.01	0.0	4.71	0.0	2.80	0.0
0.1 mW	15.00	0.0	4.71	0.0	2.80	0.0
1 mW	14.95	0.4	4.71	0.1	2.79	0.1

PZT average power to battery	200 W/m²: time (h)	200 W/m²: reduction (%)	600 W/m²: time (h)	600 W/m²: reduction (%)	1000 W/m²: time (h)	1000 W/m²: reduction (%)
10 mW	14.47	3.5	4.66	1.1	2.78	0.7
100 mW	10.99	26.8	4.23	10.3	2.62	6.4

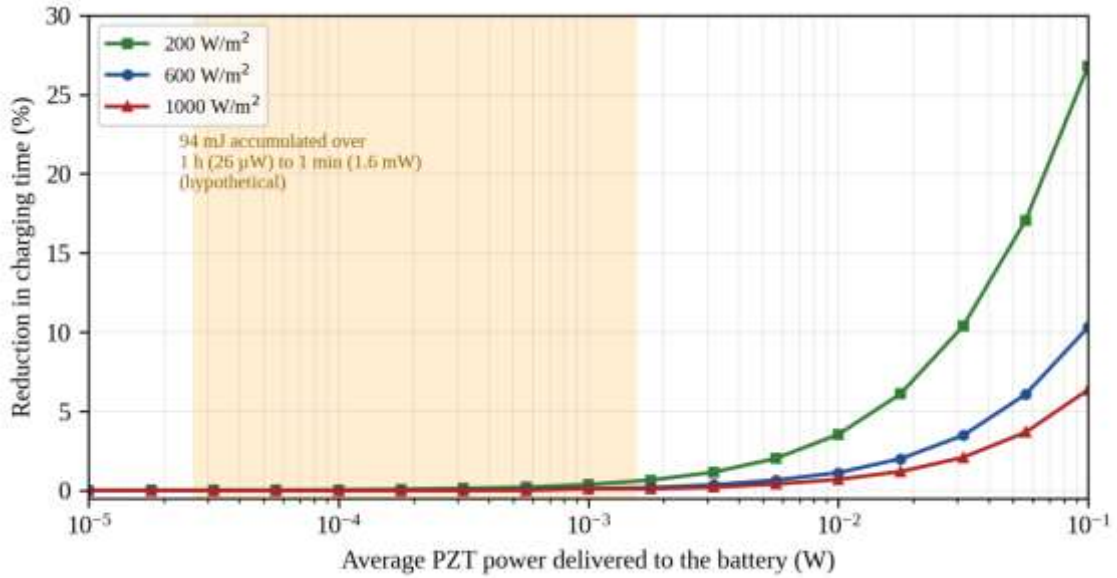


Figure 4. Simulated percentage reduction in charging time versus assumed PZT power; illustrative low-power region is hypothetical and is not derived from measured energy transfer.

A one-at-a-time parameter sensitivity analysis (Table 3) indicates that ±15% variation in the fitted PV current changes charging time by approximately −13% to +18% without the load and −18% to +29% with the load, depending on irradiance. Changing boost efficiency from 0.85 to 0.80 or 0.90 alters load-connected charging times by roughly 1%–3%; tested changes to dropout and other charger settings have smaller effects in this model. This demonstrates that uncertainties in the PV source representation may dominate small hypothetical PZT gains. The sensitivity sweep is one-at-a-time and does not establish confidence intervals or account for correlated uncertainties. The fitted PV curve is approximate, and irradiance is held constant over each simulated charge interval. Charging-time percentages should not be interpreted as statistically validated improvements.

Table 3. One-at-a-time sensitivity of simulated PV-only charging time to model assumptions.

Change	600 W/m², load off	600 W/m², load on	1000 W/m², load off	1000 W/m², load on
Baseline	4.71	6.81	2.80	3.42
PV current −15%	5.58 (+18.3%)	8.76 (+28.7%)	3.30 (+18.0%)	4.21 (+22.9%)
PV current +15%	4.08 (−13.4%)	5.57 (−18.2%)	2.43 (−13.2%)	2.88 (−15.7%)

Change	600 W/m², load off	600 W/m², load on	1000 W/m², load off	1000 W/m², load on
Boost efficiency 0.80	4.71 (0.0%)	7.01 (+2.9%)	2.80 (0.0%)	3.47 (+1.4%)
Boost efficiency 0.90	4.71 (0.0%)	6.65 (−2.4%)	2.80 (0.0%)	3.38 (−1.2%)
Dropout 0.4 V	4.74 (+0.5%)	6.86 (+0.7%)	2.81 (+0.3%)	3.43 (+0.3%)
Current limit 0.5 A	no change	no change	no change	no change
Battery resistance 0.10 Ω	no change	no change	no change	no change
Re-start threshold 4.10 V	no change	no change	no change	no change

5. Conclusions, Limitations and Future Experimental Work

5.1 Conclusion

The simulation indicates that the value of supplementing a low-power solar charging system with piezoelectric energy depends strongly on net average power actually delivered to storage. Under the stated reduced-order assumptions, a 100 mW supplementary source reduces PV-only charging time by 26.8%, 10.3% and 6.4% at 200, 600 and 1000 W/m², respectively, while 1 mW or less yields changes below 0.5%. PV-only charging is highly irradiance dependent, and PV-current uncertainty can exceed the predicted gain of a weak supplementary source. These findings support a conditional, simulation-based design insight, not a demonstrated performance improvement, physical feasibility claim or field-ready traffic-light supply. The 100 mW scenario is an imposed net electrical power at the storage boundary; the study does not demonstrate that the selected PZT discs can sustain this output. Results support a conditional feasibility and sensitivity conclusion, not experimentally demonstrated hybrid superiority.

5.2 Limitations

The main limitations are the uncalibrated ideal PZT representation, absence of measured or independently established net PZT power, simplified battery voltage–SOC and charger laws, fitted PV I–V curve, assumed fixed irradiance and load, and incomplete model files and solver settings. The original switching-level model and hour-scale reduced-order model are not identical. Parameter sweeps are deterministic and do not constitute statistical uncertainty bounds. No simulation result is validated experimentally in this article. The TP4056-type simplified model does not fully resolve constant-current/constant-voltage transition, thermal regulation, charge termination and source impedance under all operating conditions. The original 97% target is model-specific and should not be treated as a universal battery-charge limit. A direct rectifier-to-cell PZT pathway would require a safe, explicitly designed charge-management interface before physical implementation.

The assumed 0.225 W traffic-light demand is illustrative, not a measured full intersection load. The model does not quantify transducer fatigue, mechanical-to-electrical efficiency, rectifier losses, battery protection, thermal effects, and realistic traffic excitation or installation costs. These limitations restrict generalization to real roadway deployments.

5.3 Future Work

Future experimental work should construct and instrument the conceptual PV–PZT system, measure PV irradiance and temperature, and determine net PZT energy reaching storage under controlled force, displacement, excitation frequency and count. The proposed physical setup is a future validation platform, not evidence presented in the current results. A safe, characterized energy-harvesting interface and lithium-

ion charge-protection pathway must be implemented before battery-coupled tests. No experimental setup, hardware photograph or outdoor measurements are presented as study results. Hardware construction and controlled validation are exclusively future work.

Matched PV-only and PV-plus-PZT tests should use the same irradiance, load, initial battery SOC and time window, and should report current and voltage at each energy-transfer boundary, uncertainty, repeated trials and charger losses. The resulting measured net PZT power can then replace the hypothetical sensitivity scenarios. Alternative rectifier and synchronized-switch harvesting interfaces [5]–[8] and MPPT may be compared after measurement.

Future model refinement should use measured PV I–V curves, explicit PZT capacitance and source impedance, a physically realizable harvesting converter, a documented battery model and reproducible scripts with solver settings. A subsequent experimental study may evaluate battery–supercapacitor buffering, endurance, fatigue, maintenance and techno-economic feasibility [1]–[4], [20].

Suggested validation protocol: record capacitor voltage before and after N identical controlled excitations, with known capacitance C, force and elapsed time, to estimate capacitor energy change $\Delta E = \frac{1}{2}C(V_2^2 - V_1^2)$ and energy per excitation $\Delta E/N$, correcting for leakage and loading. More directly, acquire synchronized battery-interface voltage and current and integrate $E = \int v(t)\, i(t)\, dt$ to quantify net transferred energy. Then compare matched PV-only and hybrid configurations using measured battery SOC, net charge energy and load runtime. All such experiments are explicitly proposed future work.

REFERENCES

1. Z. Liu et al., “Comprehensive study on fatigue degradation of road piezoelectric energy harvesters under thermal-mechanical coupling effect,” Smart Materials and Structures, vol. 32, no. 2, Art. no. 025017, Jan. 2023, doi: 10.1088/1361-665X/acb186.
2. H. Yang et al., “Development in stacked-array-type piezoelectric energy harvester in asphalt pavement,” Journal of Materials in Civil Engineering, vol. 29, no. 11, 2017, doi: 10.1061/ (ASCE) MT.1943-5533.0002079.
3. Y. Zhang, Q. H. Lai, J. Wang, and C. Lü, “Piezoelectric energy harvesting from roadways under open-traffic conditions: Analysis and optimization with scaling law method,” Energies, vol. 15, no. 9, Art. no. 3395, May 2022, doi: 10.3390/en15093395.
4. D. Vizzari, N. Bahrani, and G. Fulco, “Coexistence of energy harvesting roads and intelligent transportation systems (ITS),” Infrastructures, vol. 8, no. 1, Art. no. 14, Jan. 2023, doi: 10.3390/infrastructures8010014.
5. Y.-C. Shu, I. C. Lien, and W.-J. Wu, “An improved analysis of the SSHI interface in piezoelectric energy harvesting,” Smart Materials and Structures, vol. 16, no. 6, pp. 2253–2264, Oct. 2007, doi: 10.1088/0964-1726/16/6/028.
6. J. Liang and W.-H. Liao, “Improved design and analysis of self-powered synchronized switch interface circuit for piezoelectric energy harvesting systems,” IEEE Transactions on Industrial Electronics, vol. 59, no. 4, pp. 1950–1960, 2012, doi: 10.1109/TIE.2011.2167116.
7. Y. Wan, Z. Chen, Y. Ye, and H. Zheng, “A synchronized switch harvesting on capacitor and inductor (SSHCI) circuit for piezoelectric energy harvesting,” IEICE Electronics Express, vol. 23, no. 5, Art. no. 20250708, 2026, doi: 10.1587/elex.23.20250708.
8. Q. Zuo et al., “An ultra-efficient and compact flipping-input synchronized switch harvesting on inductor and capacitors interface circuit for piezoelectric energy harvesting,” IEEE Transactions on

Circuits and Systems II: Express Briefs, vol. 71, no. 8, pp. 4000–4004, Mar. 2024, doi: 10.1109/TCSII.2024.3376545.
9. E. Dallago et al., "A 300-mV low-power management system for energy harvesting applications," IEEE Transactions on Power Electronics, vol. 31, no. 3, pp. 2273–2281, 2016, doi: 10.1109/TPEL.2015.2431439.
10. M. Dini, A. Romani, M. Filippi, and M. Tartagni, "A nanocurrent power management IC for low-voltage energy harvesting sources," IEEE Transactions on Power Electronics, vol. 31, no. 6, pp. 4292–4304, 2016, doi: 10.1109/TPEL.2015.2472480.
11. O. Younis and N. Moayeri, "Employing cyber-physical systems: Dynamic traffic light control at road intersections," IEEE Internet of Things Journal, vol. 4, no. 6, pp. 2286–2296, Oct. 2017, doi: 10.1109/JIOT.2017.2765243.
12. B. Diong, "Justification and conceptual design of solar-powered traffic signal systems," Oct. 2014, doi: 10.1109/ICRERA.2014.7016454.
13. A. Huda, A. M. Prasetia, and L. Sartika, "Design of a solar power system for a four-way intersection traffic light based on time scheduling using PLC," Emitor, vol. 25, no. 2, pp. 120–127, 2025, doi: 10.23917/emitor.v25i2.9159.
14. J. R. Moreira-Mendoza, M. R. Gámez, A. A. Guerrero-Vélez, J. D. Mercado-Bautista, and A. M. Hernández-Bazurto, "Independent power system for traffic lights through solar energy in Ecuador-Manabí-Portoviejo," Mar. 2025, doi: 10.21744/ijecs.v8n1.2371.
15. F. Mohammadi, A. Hajinezhad, A. Kasaeian, and S. F. Moosavian, "Effect of dust accumulation on performance of the photovoltaic panels in different climate zones," International Journal of Sustainable Energy and Environmental Research, vol. 11, no. 1, pp. 43–56, Jun. 2022, doi: 10.18488/13.v11i1.3041.
16. H. Liu, J. Zhong, C. Lee, S. Lee, and L. Lin, "A comprehensive review on piezoelectric energy harvesting technology: Materials, mechanisms, and applications," Applied Physics Reviews, vol. 5, no. 4, Dec. 2018, doi: 10.1063/1.5074184.
17. S. R. Anton and H. A. Sodano, "A review of power harvesting using piezoelectric materials (2003–2006)," Smart Materials and Structures, vol. 16, no. 3, May 2007, doi: 10.1088/0964-1726/16/3/R01.
18. N. Sezer and M. Koç, "A comprehensive review on the state-of-the-art of piezoelectric energy harvesting," Nano Energy, vol. 80, Art. no. 105567, 2021, doi: 10.1016/j.nanoen.2020.105567.
19. K. R. Komatla and S. R. Patri, "A self-start-up sub-threshold DC/DC boost converter using bootstrap driver for self-powered sensor nodes," Sep. 2021, doi: 10.13164/re.2021.0670.
20. H. Najini and S. A. Muthukumaraswamy, "Piezoelectric energy generation from vehicle traffic with technoeconomic analysis," Journal of Renewable Energy, vol. 2017, pp. 1–16, Jan. 2017, doi: 10.1155/2017/9643858.
21. M. N. Mahmud and M. N. R. Baharom, "Development of UPS for pedestrian traffic light using solar-piezo and grid power supplies," Evolution in Electrical and Electronic Engineering, vol. 3, no. 1, pp. 477–489, 2022, doi: 10.30880/eeee.2022.03.01.054.
22. M. A. D. J. Marasinghe and R. H. G. Sasikala, "Design a solar-piezoelectric hybrid street lighting system," in Proc. International Open University Research Sessions (iOURS 2022), The Open University of Sri Lanka, 2022, ISSN 2012-9912.
23. NanJing Top Power ASIC Corp., "TP4056: 1A Standalone Linear Li-Ion Battery Charger," Rev. 2.3 datasheet. Available: https://www.toppwr.com/eproduct/view.php?id=478

24. Aerosemi Technology Co., Ltd., “MT3608 High Efficiency 1.2 MHz 2 A Step-Up Converter,” manufacturer datasheet.
25. A. M. Abdal-Kadhim, K. S. Leong and N. B. Mohamad, “Evaluation of impact based piezoelectric micro-power generator,” Journal of Telecommunication, Electronic and Computer Engineering, vol. 8, no. 4, pp. 87–89, 2016.
26. O. Hussein, W. K. S. Al-jumaili, F. F. Mustafa, E. Al-Ali and M. A. Mohammed, “Hybrid energy harvesting using piezoelectric footsteps and solar panels to ensure clarity,” Results in Engineering, vol. 26, Art. no. 104945, Jun. 2025, doi: 10.1016/j.rineng.2025.104945.
27. N. X. Yan, A. A. Basari, K. S. Leong, and N. A. A. Nawir, “Piezoelectric energy harvesting system via impact and vibration – A review,” Journal of Telecommunication, Electronic and Computer Engineering (JTEC), vol. 11, no. 1, pp. 35–41, 2019.
28. K. Mou, X. Ji, J. Liu, H. Zhou, H. Tian, X. Li, and H. Liu, “Using piezoelectric technology to harvest energy from pavement: A review,” Journal of Traffic and Transportation Engineering (English Edition), vol. 12, no. 1, pp. 68–86, 2025, doi: 10.1016/j.jtte.2024.11.002.